Acta Biomaterialia 156 (2023) 75–87

Contents lists available at ScienceDirect

Acta Biomaterialia

journal homepage: www.elsevier.com/locate/actbio

Full length article

In situ formation of osteochondral interfaces through "bone-ink" printing in tailored microgel suspensions☆

Gagan K. Jalandhra[a,d,1], Thomas G. Molley[a,d,1], Tzong-tyng Hung[b], Iman Roohani[c,d], Kristopher A. Kilian[a,c,d,*]

[a] School of Materials Science and Engineering, University of New South Wales, Sydney NSW 2052
[b] Biological Resources Imaging Laboratory, Mark Wainwright Analytical Centre, University of New South Wales, Sydney NSW 2052
[c] School of Chemistry, University of New South Wales, Sydney NSW 2052
[d] Australian Centre for NanoMedicine, University of New South Wales, Sydney NSW 2052

ARTICLE INFO

Article history:
Received 14 April 2022
Revised 21 July 2022
Accepted 23 August 2022
Available online 30 August 2022

Keywords:
Bone
Cartilage
Stem cells
Tissue engineering
Bioprinting

ABSTRACT

Osteochondral tissue has a complex hierarchical structure spanning subchondral bone to articular cartilage. Biomaterials approaches to mimic and repair these interfaces have had limited success, largely due to challenges in fabricating composite hard-soft interfaces with living cells. Biofabrication approaches have emerged as attractive methods to form osteochondral analogues through additive assembly of hard and soft components. We have developed a unique printing platform that is able to integrate soft and hard materials concurrently through freeform printing of mineralized constructs within tunable microgel suspensions containing living cells. A library of microgels based on gelatin were prepared, where the stiffness of the microgels and a liquid "filler" phase can be tuned for bioprinting while simultaneously directing differentiation. Tuning microgel stiffness and filler content differentially directs chondrogenesis and osteogenesis within the same construct, demonstrating how this technique can be used to fabricate osteochondral interfaces in a single step. Printing of a rapidly setting calcium phosphate cement, so called "bone-ink" within a cell laden suspension bath further guides differentiation, where the cells adjacent to the nucleated hydroxyapatite phase undergo osteogenesis with cells in the surrounding medium undergoing chondrogenesis. In this way, bone analogues with hierarchical structure can be formed within cell-laden gradient soft matrices to yield multiphasic osteochondral constructs. This technique provides a versatile one-pot biofabrication approach without harsh post-processing which will aid efforts in bone disease modelling and tissue engineering.

Statement of significance

This paper demonstrates the first example of a biofabrication approach to rapidly form osteochondral constructs in a single step under physiological conditions. Key to this advance is a tunable suspension of extracellular matrix microgels that are packed together with stem cells, providing a unique and modular scaffolding for guiding the simultaneous formation of bone and cartilage tissue. The physical properties of the suspension allow direct writing of a ceramic "bone-ink", resulting in an ordered structure of microscale hydrogels, living cells, and bone mimics in a single step. This platform reveals a simple approach to making complex skeletal tissue for disease modelling, with the possibility of repairing and replacing bone-cartilage interfaces in the clinic using a patient's own cells.

1. Introduction

Osteochondral interfaces are complex matrices of varying biophysical, biochemical and cellular components. These components are organized hierarchically across an interconnected gradient from subchondral bone to articular cartilage [1–3]. As such, repair strategies have had limited success in recapitulating their micro and macro scale architecture. Osteochondral defects are

☆ Part of the Special Issue on Biofabrication for Orthopedic, Maxillofacial, and Dental Applications, guest-edited by Professors Hala Zreiqat, Khoon Lim, and Debby Gawlitta.

* Corresponding author.
E-mail address: k.kilian@unsw.edu.au (K.A. Kilian).

[1] Co-first authors.

https://doi.org/10.1016/j.actbio.2022.08.052
1742-7061/

responsible for compromised mechanical and biological integrity, and thus function of articular joints [1,4]. These defects possess poor regenerative capacity due to scarcity of vasculature and neural networks [5,6]. Left unrepaired, the damage extends to the underlying bone and leads to degenerative conditions such as osteoarthritis and intervertebral disk degeneration [4,7,8]. Current repair strategies include chondral shaving, subchondral drilling, micro-fracturing, injection of autologous chondrocytes, or mosaicplasty [9–11]. Aside from issues regarding site morbidity, fibrocartilage formation, and donor shortage, these strategies have also been reported to cause damage to surrounding tissue before having any therapeutic effect [12]. Tissue engineering holds the potential for effective, long-term treatment of osteochondral damage. A common strategy for tissue engineering of osteochondral interfaces is layering two or more scaffolds, usually made with biodegradable polymers such a PCL, collagen and fibrin glue, with different properties such as stiffness to mimic the mechanical properties of the two tissue types [8,13–16]. h-MSCs or pre-differentiated chondrocytes and osteoblasts are either seeded after binding the layers, or are seeded before, and the resulting cellular cartilage and bone layers are stitched together [17–20]. Growth factors are commonly incorporated either into the culture medium if culturing *in vitro* or to the scaffold, which allows use both *in vitro* and *in vivo*. These bi-/multi-phasic scaffold approaches are not an accurate mimic as native osteochondral interfaces do not exhibit an abrupt transition [3,8].

3D bioprinting has provided a paradigm shift in tissue engineering by allowing rapid prototyping via additive manufacturing [21–23]. Among these, embedded printing has shown great potential. Yield stress fluidity of microgels is utilized to deposit bio-inks composed of cells and/or hydrogels omnidirectionally, allowing freeform printing of 3D tissue engineering constructs [23,24]. To achieve optimal yield stress characteristics, microgels are typically packed into a jammed state whereby individual particles become trapped and unable to move freely [25]. Hinton et al. pioneered a version of this technique termed FRESH printing. Hydrogel bio-inks combined with cells were deposited inside a thermoreversible granular support bath to 3D print complex physiologically relevant structures [26].

One aspect of granular printing that has received less attention is optimizing microgels as a porous scaffolding, in which biophysical and biochemical attributes may be tailored to direct cell activity [27–29]. Microgel stiffness can be varied, and localization of microgel combinations can be tailored to provide control over local mechanical properties within a scaffold. Similarly, release kinetics of encapsulated factors or drugs can be spatiotemporally controlled, allowing better mimicry of biochemical gradients or directing localized cellular activity [30–32]. This is necessary for the fabrication of complex tissues with variations in local architecture such as the osteochondral interface [13]. Further, microgel surfaces may be modified physically or chemically, their degradation characteristics tuned, their sizes varied, and combinations of these alterations used to direct activity of integrated cells [33–35]. In this way, microgel-based scaffolds provide unprecedented control of micro-scale features in tissue engineering scaffolds for the fabrication of more accurate constructs.

Previously, we reported the development of a microgel suspension-based 3D bioprinting platform wherein any bio-ink or cell suspension could be deposited freeformly via extrusion into a cell-laden suspension [36]. The construct could then be photocrosslinked by UV light and both the deposited and integrated cells showed high viability, attachment and migration throughout the scaffold. Using this platform, we printed tumours in proximity to printed blood vessels using sacrificial inks to create a model to study cancer metastasis [36]. More recently, Roohani, Kilian, and colleagues combined this microgel-based printing system with a calcium phosphate-based “bone-ink” optimized for 3D printing, where intricate bone analogues could be deposited in the presence of living cells. We termed this technique Ceramic Omnidirectional Bioprinting in Cell-Suspensions (COBICS) and demonstrated enhanced osteogenesis when MSCs were in proximity to the calcium phosphate phase [37]. Cells far from the ink maintained their multipotent phenotype, which provides an avenue for alternative differentiation outcomes with spatial control within the construct.

In the present study, we optimized gelatin methacryloyl microgel suspensions for osteogenesis and chondrogenesis separately, by tuning stiffness of the microgels and volume of interstitial filler hydrogel between the microgels. We found that MSCs embedded in microgel suspensions with filler underwent enhanced differentiation when microgels were stiffer. Reducing the interstitial filler volume, i.e., by packing the microgels together into a jammed state, led to further enhancement of osteogenesis. MSCs in jammed microgel suspensions showed increased mineralization and Alkaline Phosphatase expression compared to suspensions with interstitial filler. Conversely, MSCs in microgel suspensions containing soft interstitial filler exhibited enhanced chondrogenesis compared to those containing no filler. Cell laden constructs showed increased compressive Young’s moduli as a function of differentiation conditions, where osteogenesis led to mineralization at the interior of the microgels and chondrogenesis led to GAG-rich matrix production. Freeform printing of a calcium phosphate bone-ink further directed differentiation with spatial control of gradient properties demonstrating the potential for “one-pot” osteochondral interfaces for tissue engineering.

2. Experimental methods

2.1. GelMa synthesis

Gelatin methacryloyl was synthesised as previously described [38]. Briefly, Gelatin Type A (Porcine, Bloom Strength 300, G2500) (Sigma Aldrich) was dissolved in PBS × 1 at 50 °C under stirring. Methacrylic anhydride (5 (v/w)% of total mixture, Sigma Aldrich) was then added and the solution was stirred for a further 90 minutes at 50°C in the dark. Thereafter, the reaction was quenched via twofold dilution with PBS × 1. The solution was subsequently centrifuged at 1000 rcf for 3 minutes, and the supernatant was dialyzed for 5 days against DI water with 14000 kDa cutoff tubes to remove unreacted reagents. The product was lyophilized for 5-7 days and stored at -20 °C.

2.2. GelMa microgel suspensions

GelMa microgels were synthesized as previously described [36]. Microgels were synthesized using a water-in-oil emulsion. Briefly, GelMa (8, 10, or 15 wt%) was first dissolved in PBS × 1at 40-55 °C. The solution was then sterile filtered (0.45 µm filter) into a stirring oil bath (Sunflower oil, Community Co.) at 40 °C and allowed to equilibrate for ten minutes (Volume ratio of GelMa:oil was 1:37). The bath was then cooled to 10-15°C and allowed to equilibrate for 25 minutes. Acetone (25 mL of acetone per 1 mL of GelMa) was added to the oil bath and allowed to stir for 60 minutes to dehydrate the microgels. They were then washed with acetone and stored in acetone at RT until needed.

To form the microgel suspensions, acetone was evaporated and the resulting dehydrated microgel powder was weighed to calculate the appropriate volumes of Dulbecco’s modified eagle medium (DMEM), 1 % wt/vol gelMA solution in DMEM and Lithium phenyl-2,4,6-trimethylbenzoylphosphinate (LAP) photoinitiator with which to hydrate them to form suspensions with the desired interstitial filler volumes. Volumes used can be calculated

Table 1
Microgel formulation to obtain suspensions with desired volume of filler.

	Volume (mL) added per 100 mg of dry microgels		
	1 % wt/vol GelMa in DMEM	Pure DMEM	LAP (2.5 wt% stock)
High Filler	3.76	0.84	0.094
Low Filler	2.20	0.80	0.063
No Filler	0	1.80	0.037

using the equations in Table 1. Microgels were hydrated for at least 12 hours before use.

2.3. Rheological analysis of microgel suspensions

Rheological analysis of the microgel suspensions was conducted using an Anton Parr Modular Compact Rheometer (MCR 302e) equipped with a 25 mm parallel plate and quartz stage. 650 µL of microgel suspension was placed on the stage and the gap was set to 1 mm. Oscillatory measurements were performed with 0.02% strain and a 1 Hz frequency for the duration of gelation at 20°C. Shear rate sweeps were performed on uncrosslinked suspensions with a 1 Hz frequency from a 0.01 to 10 shear rate (1/s) at a log ramp scale over 4 minutes. For *in situ* UV crosslinking of GelMa suspensions, a UV light (with 395nm UV light at 40 mW/cm^2 for 60 seconds, unless stated otherwise) was placed underneath to illuminate the sample through the quartz crystal stage. Strain sweep test were performed using a log ramp rate from 0.02% shear strain up to 200% at 1 Hz frequency over 8 minutes.

2.4. Compressive Young's modulus measurements of crosslinked microgel suspensions

Compression tests were performed using a universal testing instrument (ElectroPlus E1000, Instron) with a 250 N load cell (Instron). The test speed used was 1 mm/min, and samples were compressed to a 25% strain final strain. Engineering stress-strain curves were presented after tests. The strain and stress were calculated using the two equations $\varepsilon_e = \frac{\Delta h}{h_o}$ and $\sigma_e = \frac{F}{A_o}$, where h_o and A_o were the original height and cross-sectional area of the uncompressed sample, Δh was the change in height, and F was the applied force. The Young's modulus was defined as the ratio of stress to strain in the initial compression region and was determined using the average slope of fitting line within 5-10% strain region.

2.5. Quantification of interstitial filler volume

Images of the microgels were taken using confocal microscopy (Zeiss LSM 800). Then, using Fiji ImageJ, the space occupied by filler was segmented using the threshold and drawing tools. This was measured and recorded as a ratio of the overall area of the image.

2.6. Cell culture and incorporation of mesenchymal stem cells in microgel suspensions

Adipose derived mesenchymal stem cells (ADSCs) were maintained in low glucose DMEM supplemented with 1 vol% Penicillin and Streptomycin, 10 vol% Fetal Bovine Serum, and Fibroblast Growth Factor 2 (FGF-2) (10 ng/mL). All cells used within this study were between passages 5-8. For suspension cell seeding, cells were detached with trypsin, counted, centrifuged down, and resuspended to 2 × 10^7 cells/mL. Cells were then added to pre-hydrated microgel suspensions (1:20 ratio for 1 million cells per mL final concentration) and mixed thoroughly via pipetting. The cell-laden suspension was pipetted into 3D printed molds measuring 2.5 × 6 × 6 mm. Any structures were printed in the suspension at this stage with the bone-ink. The prints were locked in place by crosslinking the microgel suspension using UV irradiation (495 nm) for 90 seconds. Following this, the gels were transferred to 24-well tissue culture plates (Corning), covered with complete DMEM and incubated at 37 °C with 5% CO_2.

After 24 hours, medium was changed to either fresh DMEM, complete osteogenic medium (StemPro® Osteogenesis Differentiation Kit, A10072-01) supplemented with 1% Penicillin-Streptomycin, complete chondrogenic medium (StemPro® Chondrogenesis Differentiation Kit, A10071-01) supplemented with 1% Penicillin-Streptomycin, or a 1:1 vol:vol mix of complete osteogenic and chondrogenic mediums supplemented with 1% Penicillin-Streptomycin. The medium was changed every third day as per manufacturer's instructions. At days 7 and 21, samples were fixed with 4 wt% paraformaldehyde (PFA) (Chem-Supply) for 1-4 days at RT.

2.7. Immunofluorescence staining and tissue culture

Clearing solutions were prepared as done previously with slight modifications [39,40]. Briefly, Cubic solution 2 was prepared by mixing 50 wt% sucrose (Sigma Aldrich, 584173), 25 wt% urea, 10 wt% triethanolamine (Sigma Aldrich, 90278-100mL) with DI water at 55°C until also fully dissolved. The samples were rinsed with PBS × 1 followed by 3 PBS × 1 washes at 2–4-hour intervals (standard washing procedure). A 0.5 wt% solution of Triton x-100 in DI water was added to the gels and allowed to sit at RT overnight. The gels were then rinsed with PBS followed by 3 washes with 3 wt% bovine serum albumin (BSA) in PBS for blocking (2-hour wash intervals). Primary antibody solutions were prepared in a 3 wt% BSA solution with the dilution factors in Table S1, and the solution was added to cells on a rocker overnight at room temperature. The gels were again rinsed and washed 3 times with 3 wt% BSA in PBS. Then a secondary antibody solution was made with the addition of Hoechst (1:1000) and 488 or 647 Phalloidin (1:200). The staining solution was then added and kept overnight at room temperature under rocking. The gels were washed with PBS three times before addition of the Cubic 2 clearing solution for 2-5 days. All confocal imaging was performed with a Zeiss LSM 800. A 10x objective with a 2.5mm working distance was used to see deeper into the samples. Samples were coated with clearing 2 solution [41] throughout the duration of the imaging to prevent drying.

2.8. Cell volume segmentation analysis and cell counting analysis

Confocal z-stacks (10x objective, 51 slices over 100 µm) were taken of representative regions in each gel. 1 z-stack was taken on each replicate. The images were imported in Imaris 9.5.1 for analysis. Cell segmentations were created using the Cell module with the phalloidin stain as the cell body and Hoechst for the cell nuclei. Each z-stack was analyzed using identical thresholding values per gel with each independent nucleus as a seed for the cells. Cell statistics from each of the three replicates were pooled together for total cell morphometric analysis.

2.9. Histological stain for differentiation analysis

Alcian Blue staining assay was performed to evaluate proteoglycan synthesis. Samples were washed thrice with PBS × 1, then treated overnight at 4 °C in a 1 wt/vol% Alcian Blue 8GX (Sigma Aldrich, A5268-10G) solution in 0.1M hydrochloric acid (HCl). Following this, samples were washed thrice with 0.1M HCl, allowing at least 1 hour between each wash. The pH was neutralized with

DI water and washed 5 times to remove unreacted staining solution. Gels were photographed using a DSLR camera (Nikon D3400) and Leica M420 macroscope at 25x magnification ensuring constant lighting conditions. At least 3 images were taken of each sample and the stain intensity was quantified using Image-J (Fiji).

For sGAG quantification via dimethyl-methylene blue (DMMB) assay (Sigma Aldrich, 341088), the microgel constructs were cultured for 21 days in growth medium, osteogenic medium, or chondrogenic medium. Samples were then washed with PBS × 1 twice and digested for 18 hours with proteinase-k (0.1 mg/mL) (Sigma Aldrich, P2308) at 56°C. The solutions were then brought to 95°C for 5 minutes to deactivate the protease. A DMMB solution was prepared in glycine, NaCl and 0.1M acetic acid. 40 uL aliquots of samples were added into wells of a 96-well plate before a 160 uL solution of DMMB was directly added. Four biological replicates were used for each condition, and three technical replicates per biological replicate. Absorbance of the digested microgel solutions was taken at 525 nm immediately after. A standard curve of absorbance was simultaneously generated using known concentrations of a standard chondroitin sulfate solution (Fig. S11).

For alkaline phosphatase activity (ALK), a 5-bromo-4-chloro-3-indolyl-phosphate/ nitro blue tetrazolium BCIP/NBT tablet (Sigma Aldrich, B5655) was dissolved in DI water via sonication. The BCIP/NBT solution was then added on top of microgel slices and allowed to incubate for 18 hours. The gels were subsequently washed with DI water 5 times before imaging on a brightfield microscope with a 10x objective. Gels were again photographed using a DSLR camera (Nikon D3400) and Leica M420 macroscope at 25x magnification ensuring constant lighting conditions. At least 3 images were taken of each sample and the stain intensity was quantified using Image-J (Fiji).

For mineralization staining via Alizarin Red, microgel constructs with no or high filler were cultured for 21 days in growth or osteogenic medium. Samples were then fixed overnight in 4% PFA prior to extensive PBS × 1 washes. Alizarin red was subsequently dissolved in a solution of DI water (4 mM) and the pH was balanced to around 4 using concentration ammonium hydroxide. The solution was then sterile filtered (0.22 μm) and added a 24 well plate with the samples. After 10 minutes, the samples were washed with PBS 7 times and left to sit in a sodium acetate buffer (0.1M pH 5) for 4 hours before imaging with a Pixel 4A phone camera and Nikon light microscope.

2.10. MicroCT of mineralization

The gels were sealed in parafilm and placed on the mouse holder for MicroCT imaging. MicroCT images for the gels were acquired at 50 KV, 0.24 mA, 75 ms exposure, 360 degrees and 720 projections with the Milabs U-CT scanner (Houten, Netherlands) under mouse total body accurate settings. The images were reconstructed with Milabs.Rec 10.16 software at 30 micrometer voxel size. The MicroCT data was analyzed with Inveon Research Workplace 4.2 (Siemens, Australia). Dicom data was loaded into the Multimodal 3D visualization module and segmented manually. The extent of calcification with Hounsfield unit (HU) greater than 300 or 1000 was applied to each gel and the volume and surface area computed with the statistics function.

2.11. Ceramic ink synthesis

The ceramic bone ink was synthesized as previously described [37]. Briefly, calcium hydrogen phosphate ($CaHPO_4$) (Sigma Aldrich, C7263) and calcium carbonate ($CaCO_3$) (Sigma Aldrich, 310034) were combined in a 3:2 Ca:P molar ratio, then heated in an alumina crucible to 1400°C for 4 hours before being quenched to form α-TCP. Once completely cooled, the solid was crushed with a mortar and pestle before being ground to a fine powder using a planetary ball mill in two stages – first, for two hours with zirconia balls with a diameter of 10 mm, then for two hours with zirconia balls with a diameter of 1 mm. Ethanol was used to wash between the ball milling stages and to suspend the powder while ball milling. Between and after the ball milling stages, α-TCP was dried by heating in an oven at 100°C for 24 hours. The ink was characterized using Raman spectroscopy and X-Ray Diffraction to ensure formation of the desired phase. To confirm formation of the correct phase of TCP, a batch of ink was formulated as detailed below and printed into a bath of deionized water. Adequate purity would mean the ink hardens after approximately 6 minutes.

To form the ink for printing, α-TCP powder was combined with glycerol (Sigma Aldrich, G9012), polysorbate 80 (Sigma Aldrich, P1754), and ammonium phosphate dibasic (Sigma Aldrich, A5764) and ball milled for 60 minutes with a 25 mm diameter zirconia ball to homogenize the ink. Measurements used are provided in Table S2. The ink was loaded into a 1 mL syringe fitted with a needle with the desired nozzle size for printing.

2.12. Fidelity of ceramic ink prints

Once loaded into a syringe (Livingstone, DSL001MLS) fitted with a needle (Nordson EFD 22GA), the ceramic bone ink was printed into microgel suspensions with no filler, low filler, and high filler volumes. The constructs were photo-crosslinked using a UV lamp and imaged via brightfield microscopy. Analysis was performed using ImageJ. Diameter was measured at 6 points along the length of the printed ink in each construct.

2.13. NMR characterization of GelMa Methacrylation

The degree of functionalization (DOF) was quantified using a ^{1}H NMR spectrometer (Bruker Advance III 400 MHz) by referencing 1H NMR chemical shifts to the residual solvent peak at 4.80 ppm in deuterium (D2O). Briefly, 10 mg of GelMa was dissolved in 1 mL of D2O at 37°C. 700 μL was put into an NMR tube for the acquisition of the NMR data. NMR spectra were analyzed using MestreNova (Mestre lab Research) using the chemical shift in the aromatic region as integral reference. Degree of functionalization of 40% can be seen in Fig. S1. H NMR (400 MHz, D2O,): δ 7.24 (m), 5.65 (m), 5.40 (m).

2.14. Statistical analysis

All whiskers in box plots are one standard deviation (s.d.). Statistical significance was determined using a one-way ANOVA with Tukey's Post Hoc HSD analysis. Differences were considered significant when $P < 0.05$. Statistical significance was highlighted in Fig.s with the following convention: * = $P < 0.05$; ** = $P < 0.01$; *** = $P < 0.001$ (Fig. 1).

3. Results and discussion

3.1. Tuning microgel mechanical properties

To render a suspension of gelatin-based microgels stable to cell culture conditions, a crosslinking method is necessary. Previously, we demonstrated gelatin microgel stabilization through glutaraldehyde treatment [37] or through the use of methacrylated gelatin (GelMa) prior to fabrication [36]. For this work, we selected GelMa since varying either the degree of methacrylation or the weight fraction can tune the bulk mechanics of hydrogels [42]. First, GelMa was synthesized with a degree of functionalization of 40% (Fig. S1). To make the microgels, liquid GelMa was added

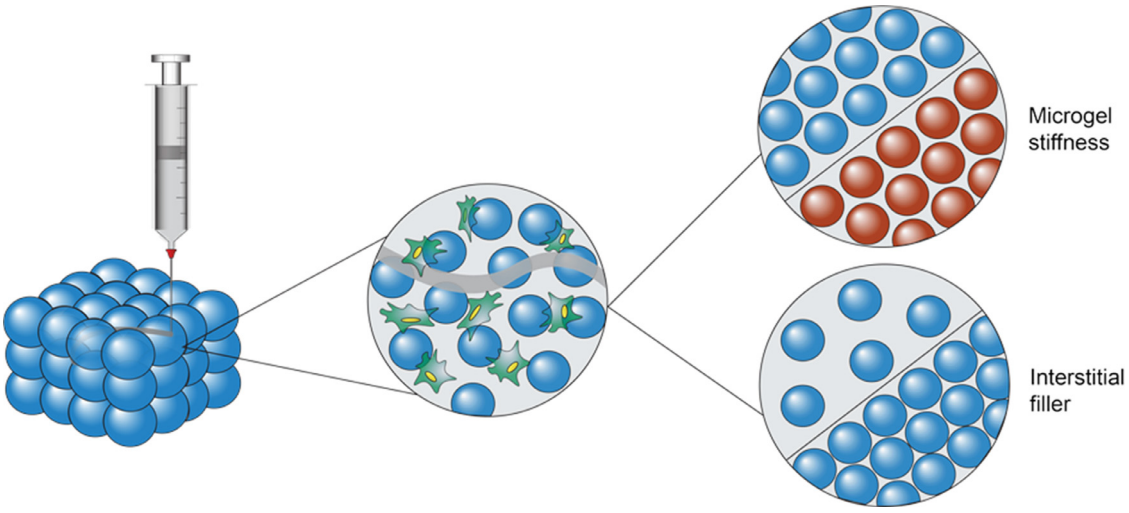

Fig. 1. A schematic of our microgel suspension based bioprinting technique. The suspensions can be laden with cells and a bio-ink (bone-ink used in the present study) deposited omnidirectionally. Properties of the microgels, i.e. stiffness (illustrated by varying colours), and the suspension, i.e. volume of interstitial gelMa filler, are varied to direct cellular activity.

dropwise to 40°C oil under stirring followed by cooling to 10°C to create stabilized triple helices and other noncovalent crosslinks [43]. Subsequent treatment with acetone dehydrated the microparticles for easy washing, weighing, and storage (Fig. 2**A**). This created particles with a mean diameter of 116 ± 38 μm (Fig. 2**B**). The mechanical properties of GelMa microgels were tuned by altering the weight percentage of the polymer solution added to the oil. Higher weight percentages lead to higher chain densities, where increased chain interactions result in changes in mechanical properties. Using this approach, we fabricated GelMa microgels with a stiffness range of 25 to 125 kPa (Fig. S2). To verify gel stability at physiological conditions, a temperature sweep from 20°C to 27°C was performed on 8wt% microgels suspensions which showed only a 10% decrease in storage modulus (Fig. S3).

For 3D printing suspension baths, and jammed suspensions in general, controlling the packing fraction is critical for controlling suspension stability and function. To aid in batch-to-batch reproducibility of microgel suspensions, dried particles were weighed and resuspended with a specific ratio of cell media, photocrosslinking solution (0.05wt% final of LAP), and a 1 wt% GelMa solution (Table 1). The addition of 1 wt% GelMa aids in suspension stabilization, handleability, printability within the jammed suspension, and crosslinking to produce a microporous scaffold. By varying the ratios of cell media and 1 wt% GelMa, microgel suspensions with varied amounts of interstitial filler were fabricated (Fig. 2**C**). Using parallel plate rheology, strain rate sweeps were performed on microgels suspensions with no filler, low filler, and high filler content. As the amount of filler increased, the viscosity of each sample decreased with a 1000-fold difference between the no filler and high filler conditions ($P < 0.0001$) (Fig. 2**D**). All three conditions showed similar shear thinning behavior (the slope of shear rate vs viscosity) which demonstrates the utility of these microgel suspensions for freeform bioprinting. When exposed to UV light (395 nm at 20 mW/cm^2 for 60 seconds), all microgel suspensions were fully crosslinked within 5 minutes, reaching stiffnesses of 1.6 ± 0.5 kPa, 3.2 ± 0.7 kPa, and 4.5 ± 0.7 kPa for the high filler, low filler, and no filler conditions, respectively. While no statistical differences were found for the low and no filler conditions ($P = 0.095$), the high filler was softer than each (High - Low: $P = 0.049$; High - None: $P = 0.003$). This is likely due to the high-volume fraction of soft filler material, as seen in Fig. 2**C**. This data also corresponds with the lower viscosities on the shear rate curves.

Parallel plate rheology was performed on microgel suspensions composed of microgels with varied stiffness (8, 10, and 15 wt% GelMa). Regardless of the percentage of filler content, all three stiffness gels had similar properties (Fig. S5), with or without filler. All stiffness groups showed similar shear thinning characteristics (Fig. S5A-B); however, 10 wt% gels had lower viscosities compared to the 8 and 15 wt% gels without filler. However, while there is a small difference between the microgel suspension viscosities of the 3 different stiffnesses with filler, these differences are not statistically significant (8-10 wt% $P = 0.270$; 10-15 wt% $P = 0.513$) (Fig. S5B). Notably, the no filler gels had roughly twice the viscosity of their low filler counterparts throughout the shear rate range, corroborating the data from Fig. 2**D**. For the shear amplitude sweeps, low filler gels had no statistical difference in yielding profiles and yield points, while the 0% filler conditions had different yield points (Fig. S5C & D). For time sweeps, all gels followed the same kinetics for crosslinking (Fig. S5E & F). For both filler and no filler, the 10 wt% gels also had a lower overall storage modulus, which is consistent with a lower initial viscosity.

3.2. Microgel stiffness influences the degree of osteogenesis in adipose-derived stem cells

Substrate mechanical properties have been shown to play a significant role in MSC differentiation. Seminal work by Discher and colleagues demonstrated how MSCs match lineage specification to the perceived stiffness of their substratum [44]. Extensive work has followed showing that MSC differentiation can be directed by matrix mechanical properties across a broad range of lineages [41,45,46]. For instance, MSCs showed increased adipogenesis on soft substrates (<10 kPa), with enhanced osteogenesis on stiffer substrates (>20 kPa). However, these trends become more complicated when moving into 3D. For instance, while soft 3D substrates have been shown to promote adipogenesis and stiffer substrates shown to promote osteogenesis, a biphasic osteogenic response to the properties of the microenvironment is seen in 3D hydrogels unlike 2D hydrogels [47]. Huebsch et al. demonstrated how fate decision to osteogenic lineages improved as stiffness increased to 30 kPa, but the effect quickly tapered off beyond 40 kPa [48]. This result supports the idea of 'lineage-specific' optimal mechanical properties.

To assess if the stiffness of microgel particles influences ADSCs, one million cells per mL were added to suspension of 8, 10, and

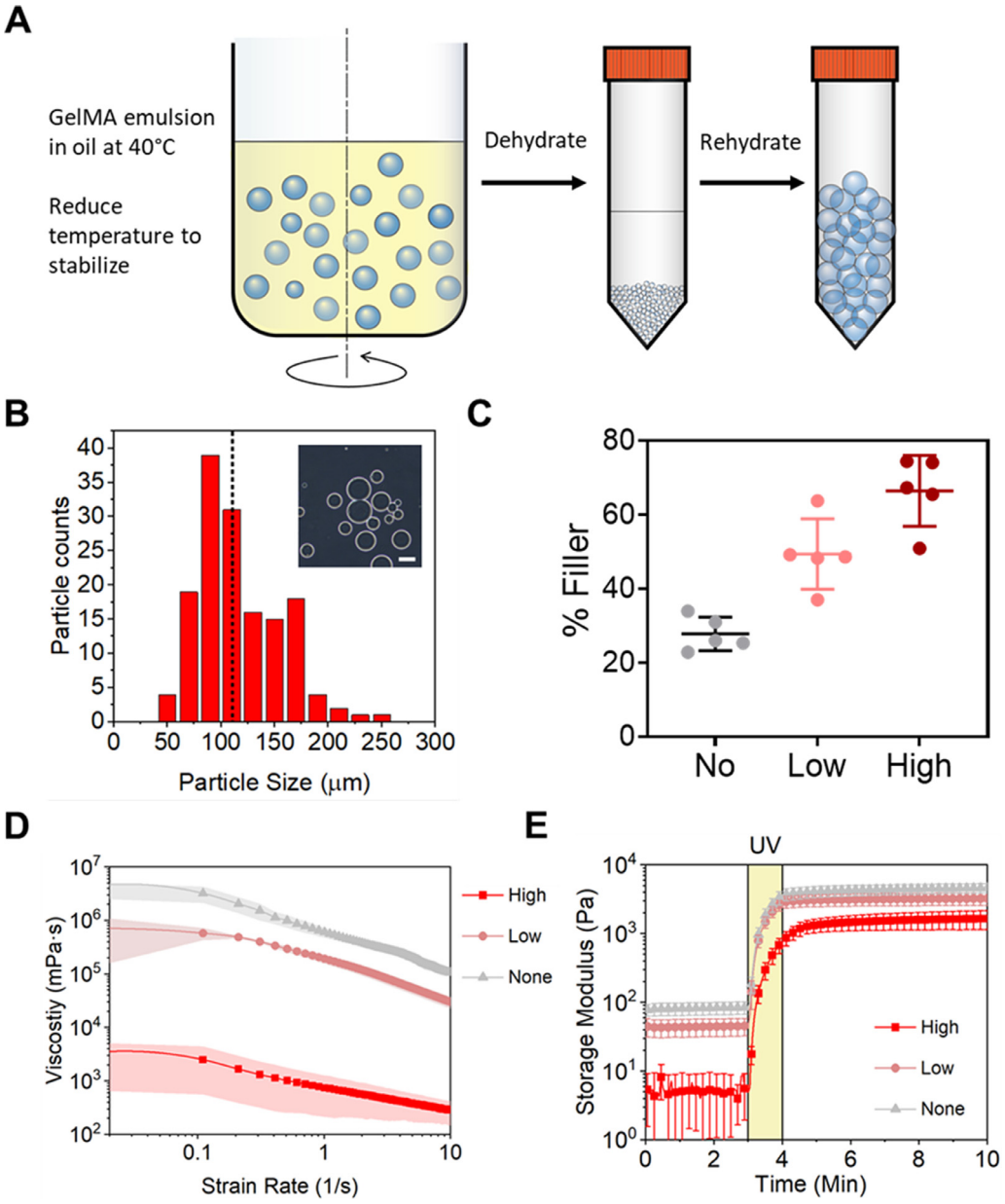

Fig. 2. Characterization of microgels used for suspension matrices. A) A schematic depicting our printing methodology. B) Size characterization histogram (N = 150 particles) and an optical image of hydrated microgels (inset). C) Plot of global porosity of microgel suspensions with high, low, and no filler. D) Rheological viscosity vs shear strain rate plot from shear strain sweeps for high, low, and no filler microgel suspensions (log ramp from 0.02-10 s-1). E) Crosslinking time sweeps conducted on a rheometer (UV (395 nm) initiated after 3 minutes, 0.2% oscillatory shear strain, 1Hz) for microgel suspensions with high, low, or no filler. Scale Bars: 100 μm.

15 wt% suspensions for 1, 3, and 7 days (Fig. 3**A**). Greater cell proliferation was observed at Day 7 in 8 wt% suspensions (1.9 ± 0.2 ×) compared to 10 wt% (1.4 ± 0.03 ×) and 15 wt% (1.4 ± 0.2 ×) relative to Day 1 when treated with osteogenic medium (Fig. 3**B**). There was a statistically significant increase in cell proliferation compared to Day 1 in the 8 wt% suspensions ($P = 0.0096$). Initial morphometric analyses show that 8 and 10 wt% particle conditions had an increase in cell volume for days 3 (8wt%: $P = 0.0018$; 10wt%: $P < 0.0001$) and 7 (8wt%: $P < 0.0001$; 10wt%: $P < 0.0001$) when compared to day 1, while the 15 wt% condition only had a difference after 7 days (Day 1 - Day 3: $P = 0.48$; Day 1 – Day 7: $P < 0.0001$) (Fig. 3**A**, 3**C**). No statistically significant differences between the groups in cell volumes were found after the first 3 days. However, by day 7, the stiffest group had cell volumes 14% higher than medium stiffness group (7400 μm^3 vs 8450 μm^3; $P = 0.065$), and 27% higher than softest group (6600 μm^3 vs 8450 μm^3; $P = 0.000015$). For cell sphericity, each condition led to a decrease in cell sphericity as time went to 3 and 7 days of culture (Fig. 3**D**). Cells encapsulated in the 8 wt% condition were significantly less round compared to the 10 wt% ($P < 0.0001$) and 15 wt% ($P < 0.0001$) conditions at day 1. These results show how ADSC shape characteristics—a hallmark parameter for predicting lineage specification—can be tuned by adjusting the stiffness of the microgels [49,50].

We next tested whether these morphometric differences would correspond to changes in the degree of osteogenesis. Cell laden microgel suspensions of all three stiffnesses, containing 1 wt% filler, were exposed to osteogenic media for 7 or 21 days. Initial morphometric analyses on day 7 show a higher cell volume for the 10 wt% condition (8 vs 10%: $P < 0.0001$; 15 vs 10%: $P < 0.0001$) with os-

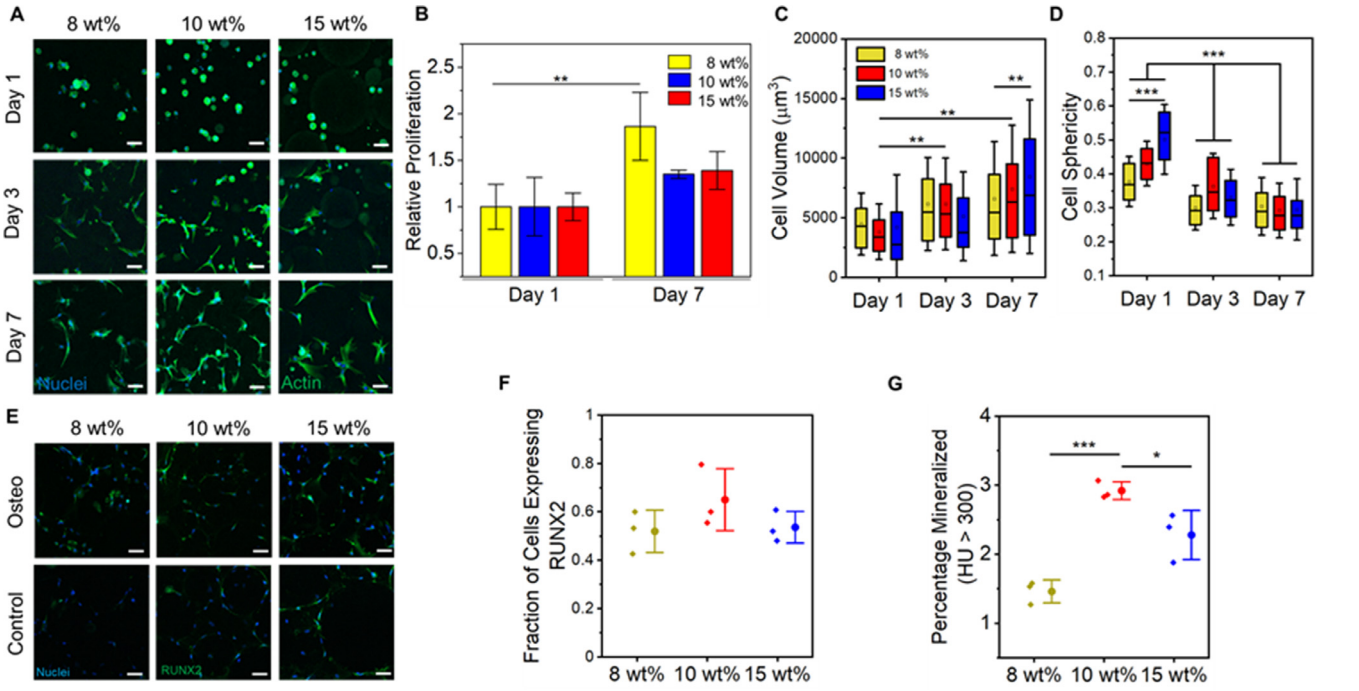

Fig. 3. The role of microgel stiffness on osteogenic differentiation. A) Confocal z-stack projection images (51 slices over 100 μm) of nuclear and actin stains for ADSCs seeded in microgels of 8 wt%, 10 wt%, and 15 wt% over 1,3, and 7 days. B) Relative (to Day 1) proliferation of ADSCs in microgel suspensions of 8 wt%, 10wt% and 15 wt% over 7 days. Morphometric analysis plots of cell volume (C) and cell sphericity (D) of cells in microgel suspensions with varied stiffness particles. E) Confocal z-stack projection images (51 slices over 100 μm) of nuclear, actin, and RUNX2 stained ADSCs seeded in microgels with 8, 10, and 15 wt% particles after 7 days in control or osteogenic media. F) Plot of fraction of cells with Nuclear RUNX2 after 7 days of differentiation in osteogenic media. G) Percentage of microgel matrices with density higher than 300 Hounsfield values (from MicroCT analyses). Scale Bars: 50 μm (A) and 100 μm (D).

teogenic media (Fig. S6A-B). Cell sphericity for the osteogenic condition was similar across all stiffnesses, with no evident trends in nuclear morphology (Fig. S6C-E). Cells were stained for RUNX2 on day 7 and the fraction of cells with nuclear RUNX2 was quantified (Fig. 3**E-F**). While there was no apparent difference in nuclear morphometrics or RUNX2 staining, by day 21 there was considerable difference in gel mineralization. The 10 wt% condition had approximately 100% and 30% more mineral than the 8 wt% ($P = 0.0007$) and 15 wt% ($P = 0.034$) conditions respectively (Fig. 3**G**). Taken together, our three stiffnesses had a biphasic osteogenesis response to matrix stiffness, similar that shown in previously [47]. However, on balance, our softest material led to the least osteogenic differentiation compared to two stiffer conditions. Overall, this data suggests that moderate stiffness gels provided a matrix more conducive to osteogenesis.

3.3. Absence of an interstitial matrix enhances osteogenic lineage specification

Cells dispersed in microgel suspensions with filler take multiple days to migrate from the interstitial space to the particle surface to initiate spreading (Fig. 3**A**, 3**C**, S6). In addition to matrix mechanics influencing stem cell fate decisions, MSCs have been shown to maintain a mechanical memory where initial adhesion to soft or stiff substrates increases the susceptibility of a cell to corresponding lineages, even when matrix mechanics are subsequently altered [51,52]. Wei et al. have recently reported that when dynamically altering a matrix from soft to stiff, MSCs had a delay in osteogenic differentiation by 5-7 days when compared to cells on statically stiff gels [53]. We have shown how individual particles can have a stiffness close to 50 kPa, while the integrated filler is 50 × softer [36]. Therefore, we hypothesized that seeding cells within the initially soft filler would influence osteogenic differentiation. To test this hypothesis, we assessed the role of filler fraction during osteogenic differentiation in microgel suspensions.

Cells were loaded within microgel suspensions with high filler, low filler, or no filler content. Cells showed significantly greater proliferation in the no filler condition by Day 7 ($P = 0.0038$). No increase was observed in the high and low filler conditions (Fig. 4**A**). By day 21, extensive mineralization was observed in the no filler condition when cultured with osteogenic medium via Alizarin Red staining (Fig. 4**B**). Quantification of the stain intensity revealed a 2.5 × more intense Alizarin Red staining in the no filler condition compared to the high filler when treated with osteogenic medium ($P = 0.029584$) (Fig. 4**C**). There were no significant differences between any of the other conditions. MicroCT scans at Day 21 show extensive mineralization in the 0% filler condition, making the gels completely opaque (Fig. 4**D**). The no filler condition had a 20-fold increase in mineral content when compared to the high filler condition, and a 12-fold increase when compared to the low filler condition (Fig. 4**E**). This difference is striking when compared to only the 2-fold increase in mineralization between 8 and 10 wt% particles (Fig. 3**G**). However, the degree of mineralization was highly variable (1 vs 0%: $P = 0.21$; 0.5 vs 0%: $P = 0.23$). These results show how integrating ADSCs into microgel suspensions with no filler phase allows immediate adhesion to the stiff particles, thereby enhancing the degree of osteogenesis.

We next assessed how varied stiffness microgels would influence osteogenesis when there was 0 filler. Day 21 MicroCT scans revealed that the 8 wt% condition showed the highest mineralization, with a 3-fold and 13-fold increase relative to the 10% ($P = 0.019$) and 15wt% ($P = 0.003$) conditions respectively (Fig. 4**F**). This is in contrast to only a 2-fold difference in relative mineralization between 8 and 10 wt% conditions when there are high levels of filler (Fig. 3**G**). Due to these larger differences, day 21 samples were subsequently stained for osteocalcin, a late-

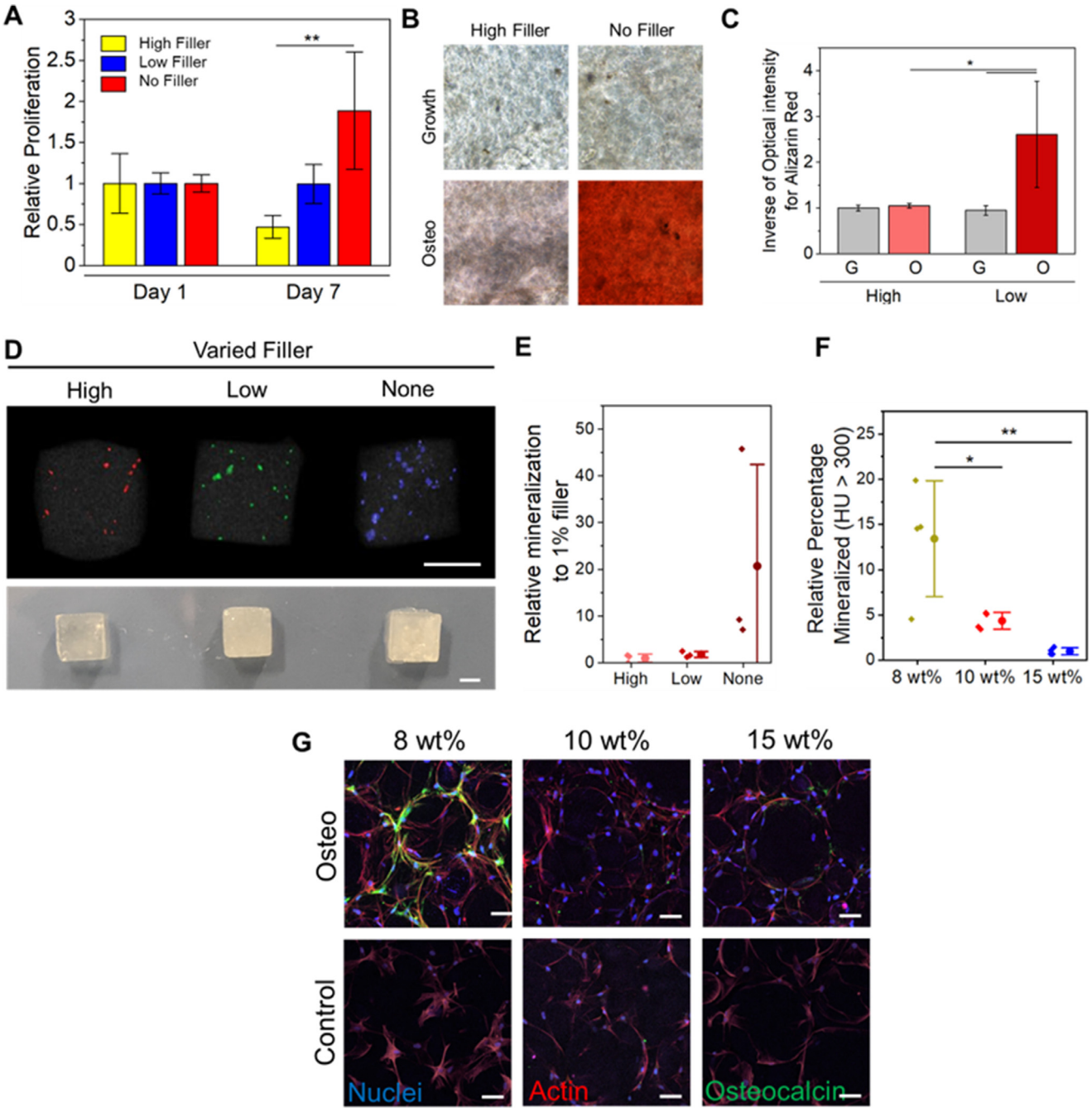

Fig. 4. Cell-laden microgel suspensions of varied filler percentages exposed to osteogenic media for 21 days. A) Relative (to Day 1) proliferation of ADSCs in microgel suspensions with high (yellow), low (blue) and no (red) filler when given osteogenic supplements. B) Optical images of ADSC-laden microgel suspensions containing high and no filler stained with Alizarin Red after 21 days of culture with growth and osteogenic media. C) Inverse Optical Intensity of ADSC-laden microgels with high and no filler stained for Alizarin Red after 21 days of culture with growth and osteogenic media. D) MicroCT segmentation analysis (top) for volume regions with a density higher than 300 Hounsfield values for the 1% filler (red), 0.5% filler (green), and 0% filler (blue). Photographs of the mineralized microgels (bottom). E) Relative percentage of microgel matrices with density higher than 300 Hounsfield values (from MicroCT analyses). F) Relative percentage of microgel matrices with density higher than 300 Hounsfield values (from MicroCT analyses). G) Confocal z-stack projection images (51 slices over 100 μm) of nuclear, actin, and Osteocalcin stained ADSCs seeded in microgels with 8, 10, and 15 wt% particles after 21 days in control or osteogenic media. Scale bars: 50 μm (D), 3 mm (A).

stage marker for osteogenesis [54]. When staining gels, osteocalcin was found only in the 8 wt% osteogenic media condition, corresponding with the mineralization data (Fig. 4**GD**). This data agrees with previous studies showing high osteogenesis around 20-30 kPa [55]. Together, these results suggest that osteogenesis is driven through adhesion to rigid matrices like the stiff particles (~25 kPa) and that fraction of filler is more important in mediating osteogenesis than the microgel stiffness in these suspension baths.

3.4. Soft interstitial matrix enhances chondrogenesis

Another important lineage for repairing musculoskeletal defects is cartilage, and there are numerous examples of scaffolding that augment chondrogenesis. Having identified optimal matrix conditions for osteogenesis, we next aimed to evaluate chondrogenesis for ADSC laden microgel suspensions. The data for osteogenesis suggests that filler plays a more important role than particle stiffness for differentiation outcomes. In addition, having an increased

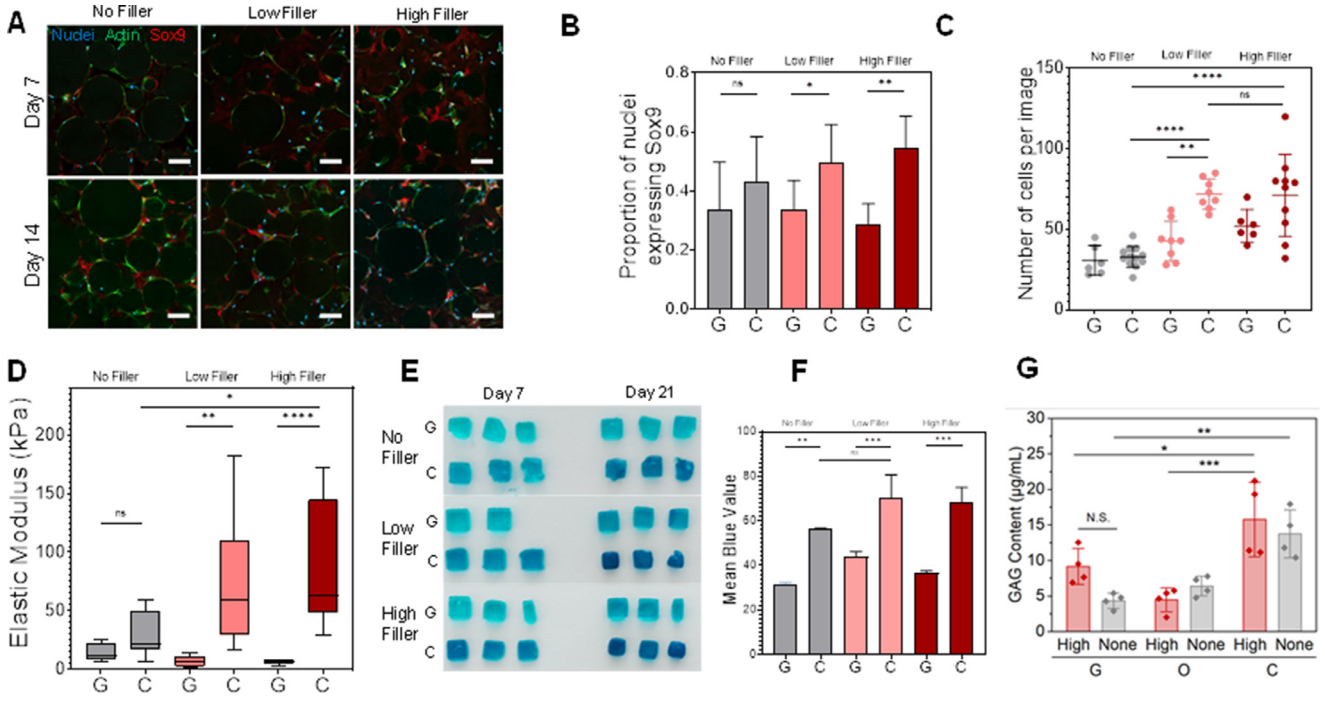

Fig. 5. Chondrogenesis of ADSCs in microgel suspensions with varying amounts of filler over 21 days. A) Immunofluorescence images of ADSCs in microgel suspensions containing no filler (top left, bottom left), low filler volume (top center, bottom center), and high filler volume (top right, bottom right) showing nuclei (blue, DAPI), actin (green, phalloidin) and chondrogenic marker Sox9 (red). B) Proportion of nuclei expressing the chondrogenic marker Sox9 in no filler (grey), low filler (peach) and high filler (red) microgel suspensions after 21 days of culture in growth (G) and chondrogenic (C) medium. C) Cell proliferation in no filler (grey), low filler (peach) and high filler (red) microgel suspensions after 21 days of culture in growth (G) and chondrogenic (C) medium presented as a cell count per image. D) Compressive Elastic Moduli of no filler (grey), low filler (peach) and high filler (red) microgel suspensions after 21 days of culture in growth (G) and chondrogenic medium. E) Alcian Blue staining of microgel suspensions after 7 and 21 days of being treated with chondrogenic (C) and growth (G) medium visualizing proteoglycan synthesis by chondrocytes. F) Quantification of the intensity of Alcian Blue stains in microgel suspensions with no filler (grey), low filler (peach) and high filler (red) after 21 days of treatment with growth (G) and chondrogenic (C) medium. G) Quantification of GAG content using DMMB assay after 21 days of culture in microgel suspensions with high (peach) and no (grey) filler when given growth medium (G), osteogenic medium (O) and chondrogenic medium (C). Scale bars: 100 µm (A).

volume of filler would facilitate greater cell-cell contacts and reduce early cell-spreading, both characteristics of early stages of native chondrogenesis (Fig. S7) [56–59]. Chondrocyte differentiation protocols typically use lower stiffness materials and high cell densities. In addition, early cartilage has a stiffness of only 15 – 25 kPa [60]. For these reasons, we focused our evaluation on the effect of filler rather than particle stiffness.

We started by culturing ADSCs in microgel suspensions consisting of the same stiffness (10wt%) microgels with systematic variations in filler content—no filler, low filler, and high filler—for 7 and 21 days. After fixation, we immunostained the samples with the chondrogenic master regulator Sox9 [61–63] to probe the effect of filler on guiding chondrogenesis. After 7 days, there were no significant differences in Sox9 expression across all conditions. However, by day 21, a greater proportion of cells in low and high filler suspensions showed nuclear expression of Sox9 when given chondrogenic supplements compared to the control medium (Fig. 5**A-B**). In suspensions with no filler, there was no significant difference between the control and chondrogenic conditions. This is in sharp contrast to the osteogenic conditions where there was considerably higher differentiation in the absence of filler. Interestingly, we saw significantly higher proliferation for cells embedded in the interstitial space when filler was present compared to the no filler condition (No filler – Low filler, p-value <0.0001; No filler – High filler, p-value <0.0001) (Fig. 5**C**). Even without chondrogenic supplements, cells showed greater proliferation in low filler (43 ± 12 cells per area) and high filler (53 ± 10 cells per area) compared to no filler (31 ± 9 cells per area). This suggests that increasing filler content stimulates proliferation and chondrogenesis.

Next, we evaluated the mechanical integrity and composition of deposited chondrogenic ECM through compression testing and Alcian Blue staining. No significant differences in matrix stiffness were found between any of the conditions on day 7 (Fig. S8). By day 21, microgel suspensions with low and high filler supplemented with chondrogenic medium both showed significantly higher compressive elastic moduli compared to the suspensions with no filler (Fig. 5**D**). Meanwhile, the no filler condition showed no statistical difference even between the control media and chondrogenic media. Furthermore, suspensions with filler possessed lower initial stiffnesses, meaning they showed a greater increase in moduli change compared to the no filler condition. Microgel suspensions with high filler had the greatest increase in compressive moduli from day 7 (24 ± 8 kPa) to day 21 (86 ± 55 kPa) compared to microgels with low filler which increased from 43 ± 12 kPa on day 7 to 73 ± 61 kPa on day 21 (Fig. S8). Microgels with no filler showed only a slight increase from 13 ± 5 kPa on day 7 to 29 ± 19kPa. This suggests that having a larger volume of filler facilitates enhanced deposition of the chondrogenic ECM which results in greater mechanical stiffness of the construct. These values still fall short of native adult human cartilage, which is around 10 MPa [64]. However, our samples were only cultured for 21 days as compared to naturally developed and repaired cartilage which can take upwards of 12 months [65]. Previous work uses tissue-engineered constructs that reported stiffness changes over 12 weeks [66] suggesting that longer culture times for our microgel suspensions would produce more biomimetic tissue mechanics.

Having identified a substantial increase in mechanical properties, we next evaluated glycosaminoglycan content in our mi-

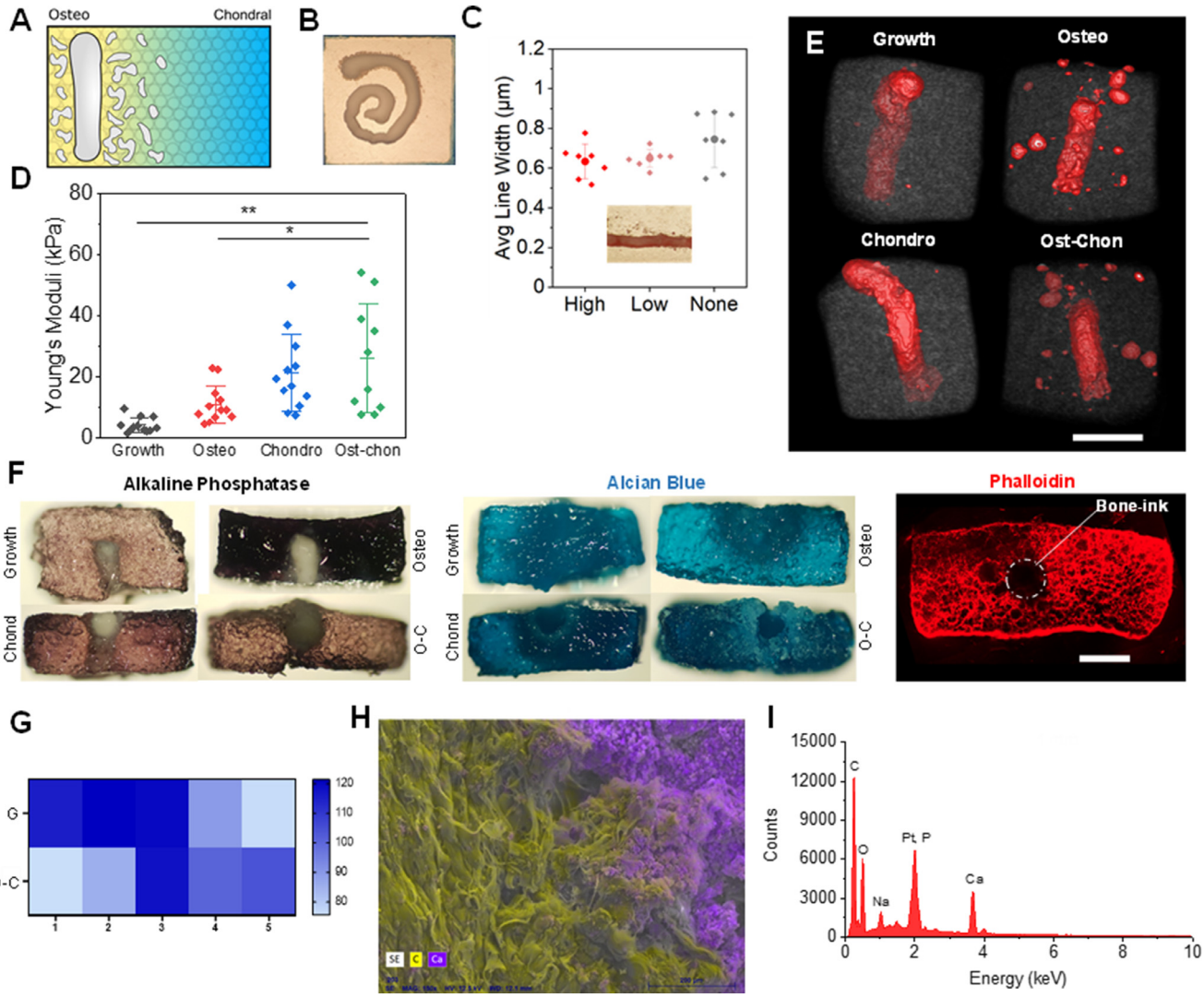

Fig. 6. Forming osteochondral interface via deposition of bone-ink in microgel suspensions. B) Macroscope image of spiral printed with bone-ink inside low filler volume microgel suspension. C) Quantification of the fidelity of structures printed with the bone-ink inside microgel suspensions with no filler (grey), low filler (peach), and high filler (red). Inset image: macroscope image of line printed with bone-ink in low filler volume suspension. D) Compressive Young's moduli of osteochondral interface constructs after 21 days of culture in growth medium (grey), osteogenic medium (red), chondrogenic medium (blue) and mixed osteo-chondro medium (green). E) MicroCT images of bone-ink line prints cultured for 21 days in growth, chondrogenic, osteogenic and osteo-chondro (O-C) mediums. F) Alkaline Phosphatase staining for osteogenesis (left) and Alcian Blue staining for chondrogenesis (center) of constructs cultured in growth, chondrogenic, osteogenic and osteo-chondro mediums on day 21. Right: Immunofluorescence image of osteo-chondro medium cultured construct after 21 days stained for actin. G) Heat map showing the intensity of Alcian Blue staining for proteoglycan synthesis as a function of distance from the ink (1 = ink, 5 = edge of gel; G = Growth medium, O-C: osteo-chondro medium). H) Scanning Electron Microscopy EDX image of the bone-cartilage interface showing the transition from calcium (purple) to carbon (yellow). I) EDX analysis of the SEM image of the interface showing the presence of carbon (Ca), phosphorus (P) and oxygen (O). Scale bars: 2mm (E), 1 mm (F).

crogel samples using Alcian Blue staining at days 7 and 21 [67–71] (Fig. 5**E**). Suspensions with low and high filler content showed a greater intensity of Alcian Blue staining at both day 7 and day 21. Quantification of stain intensity after 21 days of culture (Fig. 5**F** and S9) showed a higher value of intensity for microgels with high filler (68 ± 7, color intensity) and low filler (70 ± 11, color intensity) in chondrogenic medium compared to suspensions with no filler (56 ± 1, color intensity) under the same conditions. Suspensions with filler also showed a larger difference in stain intensity between control and chondrogenic conditions compared to microgels with no filler. DMMB assay analysis showed higher GAG content after 21 days in microgel suspensions with high filler (15.8 ± 4.5 μg/mL) compared to no filler (13.8 ± 2.9 μg/mL) when given chondrogenic medium. Both values were higher than high filler and no filler conditions treated with growth medium and osteogenic medium (Fig. 5**G**). Though the difference in GAG production between chondrogenic microgels with varying filler is not statistically significant, the higher proliferation and greater increase in elastic modulus provide evidence that higher filler content facilitates enhanced chondrogenesis.

Together, increased nuclear Sox9 expression, significantly greater proliferation, higher elastic moduli and enhanced proteoglycan-rich ECM all suggest that the presence, and volume, of interstitial filler enhances chondrogenesis in ADSC laden microgel suspensions.

3.5. Ceramic bone-ink printing for osteo-chondral interfaces

An advantage of microgel suspensions as a scaffolding for differentiation is the ability to modulate microgel and filler properties both alone and together to steer different outcomes within a single construct. Having shown that the presence of filler aids in chondrogenesis, we next aimed to deposit our previously developed bone-mimetic ink inside microgel suspensions consisting

of low volume of filler to 3D print the osteochondral interface. Low volume suspensions facilitated deposition of a chondrogenic medium for enhanced chondrogenesis and enabled mineralization when treated with osteogenic medium. Previously, we demonstrated optimization of our calcium phosphate bone-ink for extrusion printing and further demonstrated solidification within 5 minutes [37]. Nanoprecipitation of the bone-ink combined with photocrosslinking of GelMa microgels provides a double-locking mechanism to stabilize printed structures. The osteochondral interfacial construct is depicted in Fig. 6**A**, where deposition of the bone-ink will promote osteogenesis by virtue of the *in situ* hydroxyapatite phase transformation, while microgel properties away from the ink can enhance alternative lineages like chondrogenesis. By supplementing the culture with soluble triggers for both lineages, cells in proximity to the ink may undergo osteogenesis and deposit a mineralized matrix, and cells in the surrounding suspension may undergo chondrogenesis due to the presence of filler.

First, we evaluated bone-ink print fidelities in various geometries across the newly optimized microgel suspension conditions. MicroCT images of printed lines indicate that the prints are well within the microgel suspensions (Fig. S10 and supplemental video 1). As shown in Fig. 6**B** and 6**C** inset, the ink was extruded with different degrees of curvature. We investigated the consistency of prints with the bone-ink by testing the fidelity of printed structures in microgel suspensions with no filler, low filler and high filler. No significant difference was observed in the fidelity of structures printed in suspensions with varying filler content (Fig. 6**C**) while suspensions with low filler showed the greatest consistency between batches.

As proof of concept for a printed osteochondral interface, ADSCs were added to microgel suspensions, followed by printing of lines of diameter 600 µm in the center of the suspension. The structures were crosslinked and cultured in either growth medium (control), osteogenic medium, chondrogenic medium, or a 1:1 vol/vol mix of osteogenic and chondrogenic (osteo-chondro) medium. Compression testing of constructs after 21 days showed significantly larger compressive moduli for constructs cultured in chondrogenic and osteo-chondro mediums, suggesting enhanced deposition of a chondrogenic ECM for these conditions (Fig. 6**D**).

Alcian Blue staining of the of the osteo-chondro condition showed a gradient of increased proteoglycan production as a function of distance from the printed bone-ink (Fig. 6**F-G**). This suggests a gradient from cartilage to bone. No such gradient was observed in the growth medium condition. In fact, it showed slightly more intense staining towards the center, where the bone-ink was printed, but this was lower in intensity than that observed in the osteo-chondro condition. Interestingly, the chondrogenic and osteogenic conditions both showed a similar trend of increased Alcian Blue staining close to the printed bone-ink. Increased alkaline phosphatase staining in the osteo-chondro treated gels after 21 days compared to the control gels shows there is osteogenic differentiation in the interspersed ADSCs. Good proliferation of these cells was observed in the osteo-chondro treated suspensions, with consistent cell spreading throughout the gel and around the printed bone-ink. MicroCT imaging of printed lines qualitatively also show samples with increased mineral deposition in the osteo and osteo-chondro condition (Fig. 6**E** and Fig. S12). This is consistent with results reported by Romanazzo et al where osteogenic differentiation of ADSCs was enhanced in constructs containing the printed bone-ink [37]. SEM imaging combined with EDX analysis of the interface (Fig. 6**H-I**) shows an interconnected gradient from calcium of the bone ink to carbon of the microgel suspension. The attached EDX spectrum confirms the presence of calcium phosphate and carbon. Fig. S13 further shows the gradient nature of this interface. Together, these results demonstrate how printing bone analogues in optimized microgel matrices can be used to fabricate osteochondral interfaces for musculoskeletal tissue engineering.

4. Conclusions

We have presented an approach to fabricate osteochondral interfaces using tailored microgel suspensions for freeform printing of ceramic inks (COBICS) [37]. By tuning microgel stiffness and interstitial filler concentrations, we revealed how initial matrix cues are more critical than final matrix stiffness in directing stem cell osteogenic differentiation outcomes. High amounts of interstitial filler were found to enhance chondrogenesis through higher cell proliferation and matrix deposition. Pairing these outcomes with direct writing of bone analogues provides a platform with spatial control over differentiation for fabrication of gradient osteochondral tissues. Ultimately, this platform provides avenues for fine control of *in situ* formation of complex tissue interfaces, with scope for fundamental studies in tissue development as well as disease modeling and tissue engineering.

Declaration of Competing Interest

There are no conflicts of interest to declare.

The authors declare that they have no known competing financial interests or personal relationships that could have appeared to influence the work reported in this paper.

Acknowledgements

This work was supported through funding from the National Health and Medical Research Council Grant # APP1185021, the Australian Research Council Grant # FT180100417, and the National Cancer Institute of the National Institutes of Health Grant # R01CA25144. We acknowledge the help and support of staff at the Katharina Gaus Light Microscopy Facility and the Biological Specimen Preparation Laboratory of the UNSW Mark Wainwright Analytical Centre. The authors also acknowledge the facilities, and the scientific and technical assistance of the UNSW node of the National Imaging Facility. The authors acknowledge the facilities as well as the scientific and technical assistance of Sydney Imaging Core Research Facility. We acknowledge Dr. Zihao Li for assistance with NMR analysis. This research is supported by an Australian Government Research Training Program (RTP) Scholarship.

Supplementary materials

Supplementary material associated with this article can be found, in the online version, at doi:10.1016/j.actbio.2022.08.052.

References

[1] M. Oliveira Silva, J.L. Gregory, N. Ansari, K.S. Stok, Molecular Signaling Interactions and Transport at the Osteochondral Interface: A Review, Front. Cell Dev. Biol. 8 (2020).
[2] A. Di Luca, C. Van Blitterswijk, L. Moroni, The osteochondral interface as a gradient tissue: from development to the fabrication of gradient scaffolds for regenerative medicine, Birth Defects Res. C Embryo Today 105 (1) (2015) 34–52.
[3] B. Zhang, J. Huang, R.J. Narayan, Gradient scaffolds for osteochondral tissue engineering and regeneration, J. Mater. Chem. B 8 (36) (2020) 8149–8170.
[4] R. Longley, A.M. Ferreira, P. Gentile, Recent Approaches to the Manufacturing of Biomimetic Multi-Phasic Scaffolds for Osteochondral Regeneration, Int. J. Mol. Sci. 19 (6) (2018) 1755.
[5] L.-P. Yan, J.M. Oliveira, A.L. Oliveira, R.L. Reis, Current Concepts and Challenges in Osteochondral Tissue Engineering and Regenerative Medicine, ACS Biomater. Sci. Eng. 1 (4) (2015) 183–200.
[6] E. Popa, R. Reis, M. Gomes, Chondrogenic phenotype of different cells encapsulated in κ-carrageenan hydrogels for cartilage regeneration strategies, Biotechnol. Appl. Biochem. 59 (2) (2012) 132–141.
[7] C.M.E. Rustenburg, K.S. Emanuel, M. Peeters, W.F. Lems, P.-P.A. Vergroesen, T.H. Smit, Osteoarthritis and intervertebral disc degeneration: Quite different, quite similar, JOR Spine 1 (4) (2018) p. e1033-e1033.

[8] M. Liu, X. Ke, Y. Yao, F. Wu, S. Ye, L. Zhang, G. Yang, M. Shen, Y. Li, X. Yang, C. Zhong, C. Gao, Z. Gou, Artificial osteochondral interface of bioactive fibrous membranes mediating calcified cartilage reconstruction, J. Mater. Chem. B 9 (37) (2021) 7782–7792.
[9] S. Redman, S. Oldfield, C. Archer, Current strategies for articular cartilage repair, Eur. Cell Mater. 9 (23-32) (2005) 23–32.
[10] D.A. Grande, A.S. Breitbart, J. Mason, C. Paulino, J. Laser, R.E. Schwartz, Cartilage tissue engineering: current limitations and solutions, Clin. Orthop. Relat. Res. 367 (1999) S176–S185 (1976-2007).
[11] E. Kon, P. Verdonk, V. Condello, M. Delcogliano, A. Dhollander, G. Filardo, E. Pignotti, M. Marcacci, Matrix-Assisted Autologous Chondrocyte Transplantation for the Repair of Cartilage Defects of the Knee:Systematic Clinical Data Review and Study Quality Analysis, Am. J. Sports Med. 37 (1_suppl) (2009) 156–166.
[12] A. Di Luca, C. Van Blitterswijk, L. Moroni, The osteochondral interface as a gradient tissue: From development to the fabrication of gradient scaffolds for regenerative medicine, Birth Defects Res. C Embryo Today 105 (1) (2015) 34–52.
[13] X. Wang, E. Wenk, X. Zhang, L. Meinel, G. Vunjak-Novakovic, D.L. Kaplan, Growth factor gradients via microsphere delivery in biopolymer scaffolds for osteochondral tissue engineering, J. Controlled Release 134 (2) (2009) 81–90.
[14] Human Mesenchymal Progenitor Cell-Based Tissue Engineering of a Single-Unit Osteochondral Construct, Tissue Eng. 10 (7-8) (2004) 1169–1179.
[15] T. Tanaka, H. Komaki, M. Chazono, K. Fujii, Use of a Biphasic Graft Constructed with Chondrocytes Overlying a β-Tricalcium Phosphate Block in the Treatment of Rabbit Osteochondral Defects, Tissue Eng. 11 (1-2) (2005) 331–339.
[16] R.M. Schek, J.M. Taboas, S.J. Segvich, S.J. Hollister, P.H. Krebsbach, Engineered Osteochondral Grafts Using Biphasic Composite Solid Free-Form Fabricated Scaffolds, Tissue Eng. 10 (9-10) (2004) 1376–1385.
[17] B. Kreklau, M. Sittinger, M.B. Mensing, C. Voigt, G. Berger, G.R. Burmester, R. Rahmanzadeh, U. Gross, Tissue engineering of biphasic joint cartilage transplants, Biomaterials 20 (18) (1999) 1743–1749.
[18] Tissue-Engineered Fabrication of an Osteochondral Composite Graft Using Rat Bone Marrow-Derived Mesenchymal Stem Cells, Tissue Eng. 7 (4) (2001) 363–371.
[19] D. Schaefer, I. Martin, P. Shastri, R.F. Padera, R. Langer, L.E. Freed, G. Vunjak-Novakovic, In vitro generation of osteochondral composites, Biomaterials 21 (24) (2000) 2599–2606.
[20] X.X. Shao, D.W. Hutmacher, S.T. Ho, J.C.H. Goh, E.H. Lee, Evaluation of a hybrid scaffold/cell construct in repair of high-load-bearing osteochondral defects in rabbits, Biomaterials 27 (7) (2006) 1071–1080.
[21] F.L.C. Morgan, L. Moroni, M.B. Baker, Dynamic Bioinks to Advance Bioprinting, Adv. Healthc. Mater. 9 (15) (2020) 1901798.
[22] H. Liu, Y. Wang, K. Cui, Y. Guo, X. Zhang, J. Qin, Advances in Hydrogels in Organoids and Organs-on-a-Chip, Adv. Mater. 31 (50) (2019) 1902042.
[23] D.J. Shiwarski, A.R. Hudson, J.W. Tashman, A.W. Feinberg, Emergence of FRESH 3D printing as a platform for advanced tissue biofabrication, APL Bioeng. 5 (1) (2021) 010904.
[24] O. Jeon, Y.B. Lee, H. Jeong, S.J. Lee, D. Wells, E. Alsberg, Individual cell-only bioink and photocurable supporting medium for 3D printing and generation of engineered tissues with complex geometries, Mater. Horiz. 6 (8) (2019) 1625–1631.
[25] S. Torquato, F.H. Stillinger, Jammed hard-particle packings: From Kepler to Bernal and beyond, Rev. Mod. Phys. 82 (3) (2010) 2633–2672.
[26] T.J. Hinton, Q. Jallerat, R.N. Palchesko, J.H. Park, M.S. Grodzicki, H.-J. Shue, M.H. Ramadan, A.R. Hudson, A.W. Feinberg, Three-dimensional printing of complex biological structures by freeform reversible embedding of suspended hydrogels, Sci. Adv. 1 (9) (2015) e1500758.
[27] P.H. Kim, H.G. Yim, Y.J. Choi, B.J. Kang, J. Kim, S.M. Kwon, B.S. Kim, N.S. Hwang, J.Y. Cho, Injectable multifunctional microgel encapsulating outgrowth endothelial cells and growth factors for enhanced neovascularization, J. Control Release 187 (2014) 1–13.
[28] Y. Jiang, J. Chen, C. Deng, E.J. Suuronen, Z. Zhong, Click hydrogels, microgels and nanogels: Emerging platforms for drug delivery and tissue engineering, Biomaterials 35 (18) (2014) 4969–4985.
[29] E. Esposito, R. Cortesi, C. Nastruzzi, Gelatin microspheres: influence of preparation parameters and thermal treatment on chemico-physical and biopharmaceutical properties, Biomaterials 17 (20) (1996) 2009–2020.
[30] F.M. Chen, R.M. Shelton, Y. Jin, I.L. Chapple, Localized delivery of growth factors for periodontal tissue regeneration: role, strategies, and perspectives, Med. Res. Rev. 29 (3) (2009) 472–513.
[31] F.-M. Chen, R. Chen, X.-J. Wang, H.-H. Sun, Z.-F. Wu, In vitro cellular responses to scaffolds containing two microencapulated growth factors, Biomaterials 30 (28) (2009) 5215–5224.
[32] M.E. Wechsler, R.E. Stephenson, A.C. Murphy, H.F. Oldenkamp, A. Singh, N.A. Peppas, Engineered microscale hydrogels for drug delivery, cell therapy, and sequencing, Biomed. Microdevices 21 (2) (2019) 31-31.
[33] A.J. Seymour, S. Shin, S.C. Heilshorn, 3D Printing of Microgel Scaffolds with Tunable Void Fraction to Promote Cell Infiltration, Adv. Healthc. Mater. 10 (18) (2021) 2100644.
[34] A.C. Daly, L. Riley, T. Segura, J.A. Burdick, Hydrogel microparticles for biomedical applications, Nat. Rev. Mater. 5 (1) (2020) 20–43.
[35] B. Kessel, M. Lee, A. Bonato, Y. Tinguely, E. Tosoratti, M. Zenobi-Wong, 3D Bioprinting of Macroporous Materials Based on Entangled Hydrogel Microstrands, Adv. Sci. 7 (18) (2020) 2001419.
[36] T.G. Molley, G.K. Jalandhra, S.R. Nemec, A.S. Tiffany, A. Patkunarajah, K. Poole, B.A.C. Harley, T.-t. Hung, K.A. Kilian, Heterotypic tumor models through freeform printing into photostabilized granular microgels, Biomater. Sci. 9 (12) (2021) 4496–4509.
[37] S. Romanazzo, T.G. Molley, S. Nemec, K. Lin, R. Sheikh, J.J. Gooding, B. Wan, Q. Li, K.A. Kilian, I. Roohani, Synthetic Bone-Like Structures Through Omnidirectional Ceramic Bioprinting in Cell Suspensions, Adv. Funct. Mater. 31 (13) (2021) 2008216.
[38] D. Loessner, C. Meinert, E. Kaemmerer, L.C. Martine, K. Yue, P.A. Levett, T.J. Klein, F.P.W. Melchels, A. Khademhosseini, D.W. Hutmacher, Functionalization, preparation and use of cell-laden gelatin methacryloyl–based hydrogels as modular tissue culture platforms, Nat. Protoc. 11 (4) (2016) 727–746.
[39] T.G. Molley, X. Wang, T.-t. Hung, P.B. Jayathilaka, J.-L. Yang, K.A. Kilian, Geometrically Structured Microtumors in 3D Hydrogel Matrices, Adv. Biosyst. 4 (5) (2020) 2000056.
[40] Etsuo A. Susaki, K. Tainaka, D. Perrin, F. Kishino, T. Tawara, Tomonobu M. Watanabe, C. Yokoyama, H. Onoe, M. Eguchi, S. Yamaguchi, T. Abe, H. Kiyonari, Y. Shimizu, A. Miyawaki, H. Yokota, Hiroki R. Ueda, Whole-Brain Imaging with Single-Cell Resolution Using Chemical Cocktails and Computational Analysis, Cell 157 (3) (2014) 726–739.
[41] L. Gao, R. McBeath, C.S. Chen, Stem cell shape regulates a chondrogenic versus myogenic fate through Rac1 and N-cadherin, Stem Cells 28 (3) (2010) 564–572.
[42] J.W. Nichol, S.T. Koshy, H. Bae, C.M. Hwang, S. Yamanlar, A. Khademhosseini, Cell-laden microengineered gelatin methacrylate hydrogels, Biomaterials 31 (21) (2010) 5536–5544.
[43] C. Joly-Duhamel, D. Hellio, M. Djabourov, All Gelatin Networks: 1. Biodiversity and Physical Chemistry, Langmuir 18 (19) (2002) 7208–7217.
[44] A.J. Engler, S. Sen, H.L. Sweeney, D.E. Discher, Matrix Elasticity Directs Stem Cell Lineage Specification, Cell 126 (4) (2006) 677–689.
[45] G.C. Reilly, A.J. Engler, Intrinsic extracellular matrix properties regulate stem cell differentiation, J. Biomech. 43 (1) (2010) 55–62.
[46] A.S. Rowlands, P.A. George, J.J. Cooper-White, Directing osteogenic and myogenic differentiation of MSCs: interplay of stiffness and adhesive ligand presentation, Am. J. Physiol.-Cell Physiol. 295 (4) (2008) C1037–C1044.
[47] J. Hao, Y. Zhang, D. Jing, Y. Shen, G. Tang, S. Huang, Z. Zhao, Mechanobiology of mesenchymal stem cells: perspective into mechanical induction of MSC fate, Acta Biomater. 20 (2015) 1–9.
[48] N. Huebsch, P.R. Arany, A.S. Mao, D. Shvartsman, O.A. Ali, S.A. Bencherif, J. Rivera-Feliciano, D.J. Mooney, Harnessing traction-mediated manipulation of the cell/matrix interface to control stem-cell fate, Nat. Mater. 9 (6) (2010) 518–526.
[49] K.A. Kilian, B. Bugarija, B.T. Lahn, M. Mrksich, Geometric cues for directing the differentiation of mesenchymal stem cells, Proc. Natl. Acad. Sci. 107 (11) (2010) 4872–4877.
[50] M.D. Treiser, E.H. Yang, S. Gordonov, D.M. Cohen, I.P. Androulakis, J. Kohn, C.S. Chen, P.V. Moghe, Cytoskeleton-based forecasting of stem cell lineage fates, Proc. Natl. Acad. Sci. 107 (2) (2010) 610–615.
[51] C.X. Li, N.P. Talele, S. Boo, A. Koehler, E. Knee-Walden, J.L. Balestrini, P. Speight, A. Kapus, B. Hinz, MicroRNA-21 preserves the fibrotic mechanical memory of mesenchymal stem cells, Nat. Mater. 16 (3) (2017) 379–389.
[52] J. Lee, A.A. Abdeen, K.A. Kilian, Rewiring mesenchymal stem cell lineage specification by switching the biophysical microenvironment, Sci. Rep. 4 (1) (2014) 5188.
[53] D. Wei, A. Liu, J. Sun, S. Chen, C. Wu, H. Zhu, Y. Chen, H. Luo, H. Fan, Mechanics -controlled dynamic cell niches guided osteogenic differentiation of stem cells via preserved cellular mechanical memory, ACS Appl. Mater. Interfaces 12 (1) (2019) 260–274.
[54] S.C. Moser, B.C. van der Eerden, Osteocalcin—A versatile bone-derived hormone, Front. Endocrinol. 9 (2019) 794.
[55] O. Chaudhuri, L. Gu, D. Klumpers, M. Darnell, S.A. Bencherif, J.C. Weaver, N. Huebsch, H.-p. Lee, E. Lippens, G.N. Duda, Hydrogels with tunable stress relaxation regulate stem cell fate and activity, Nat. Mater. 15 (3) (2016) 326–334.
[56] P.J. Marie, E. Haÿ, D. Modrowski, L. Revollo, G. Mbalaviele, R. Civitelli, Cadherin-Mediated Cell–Cell Adhesion and Signaling in the Skeleton, Calcif. Tissue Int. 94 (1) (2014) 46–54.
[57] L. Bian, M. Guvendiren, R.L. Mauck, J.A. Burdick, Hydrogels that mimic developmentally relevant matrix and N-cadherin interactions enhance MSC chondrogenesis, Proc. Natl. Acad. Sci. 110 (25) (2013) 10117–10122.
[58] A.M. DeLise, R.S. Tuan, Alterations in the spatiotemporal expression pattern and function of N-cadherin inhibit cellular condensation and chondrogenesis of limb mesenchymal cells in vitro, J. Cell. Biochem. 87 (3) (2002) 342–359.
[59] A.M. Delise, R.S. Tuan, Analysis of N-cadherin function in limb mesenchymal chondrogenesis in vitro, Dev. Dyn. 225 (2) (2002) 195–204.
[60] M. Stolz, R. Gottardi, R. Raiteri, S. Miot, I. Martin, R. Imer, U. Staufer, A. Raducanu, M. Düggelin, W. Baschong, A.U. Daniels, N.F. Friederich, A. Aszodi, U. Aebi, Early detection of aging cartilage and osteoarthritis in mice and patient samples using atomic force microscopy, Nat. Nanotechnol. 4 (3) (2009) 186–192.
[61] H. Akiyama, Control of chondrogenesis by the transcription factor Sox9, Mod. Rheumatol. 18 (3) (2008) 213–219.
[62] X. Jiang, X. Huang, T. Jiang, L. Zheng, J. Zhao, X. Zhang, The role of Sox9 in collagen hydrogel-mediated chondrogenic differentiation of adult mesenchymal stem cells (MSCs), Biomater. Sci. 6 (6) (2018) 1556–1568.
[63] T.E. Hardingham, R.A. Oldershaw, S.R. Tew, Cartilage, SOX9 and Notch signals in chondrogenesis, J. Anat. 209 (4) (2006) 469–480.

[64] D.K. Temple, A.A. Cederlund, B.M. Lawless, R.M. Aspden, D.M. Espino, Viscoelastic properties of human and bovine articular cartilage: a comparison of frequency-dependent trends, BMC Musculoskelet. Disord. 17 (1) (2016) 1–8.
[65] D.C. Crawford, C.M. Heveran, W.D. Cannon, L.F. Foo, H.G. Potter, An autologous cartilage tissue implant NeoCart for treatment of grade III chondral injury to the distal femur: prospective clinical safety trial at 2 years, Am. J. Sports Med. 37 (7) (2009) 1334–1343.
[66] G.N. Duda, A. Haisch, M. Endres, C. Gebert, D. Schroeder, J.E. Hoffmann, M. Sittinger, Mechanical quality of tissue engineered cartilage: results after 6 and 12 weeks in vivo, J. Biomed. Mater. Res.: Off. J. Soc. Biomater. Jpn. Soc. Biomater. Austr. Soc. Biomater. Korean Soc. Biomater. 53 (6) (2000) 673–677.
[67] G. Li, B. Zheng, L.B. Meszaros, J.B. Vella, A. Usas, T. Matsumoto, J. Huard, Identification and characterization of chondrogenic progenitor cells in the fascia of postnatal skeletal muscle, J. Mol. Cell Biol. 3 (6) (2011) 369–377.
[68] J.E. Scott, J. Dorling, Differential staining of acid glycosaminoglycans (mucopolysaccharides) by alcian blue in salt solutions, Histochemie 5 (3) (1965) 221–233.
[69] A. Honarpardaz, S. Irani, M. Pezeshki-Modaress, M. Zandi, A. Sadeghi, Enhanced chondrogenic differentiation of bone marrow mesenchymal stem cells on gelatin/glycosaminoglycan electrospun nanofibers with different amount of glycosaminoglycan, J. Biomed. Mater. Res. Part A 107 (1) (2019) 38–48.
[70] P. Tanthaisong, S. Imsoonthornruksa, A. Ngernsoungnern, P. Ngernsoungnern, M. Ketudat-Cairns, R. Parnpai, Enhanced Chondrogenic Differentiation of Human Umbilical Cord Wharton's Jelly Derived Mesenchymal Stem Cells by GSK-3 Inhibitors, PLoS One 12 (1) (2017) e0168059.
[71] J.H. Galarraga, M.Y. Kwon, J.A. Burdick, 3D bioprinting via an in situ crosslinking technique towards engineering cartilage tissue, Sci. Rep. 9 (1) (2019) 19987.